# Forward and Backward Leaky Wave Radiation With Large Effective Aperture From an Electronically Tunable Textured Surface

Daniel F. Sievenpiper, *Senior Member, IEEE*

***Abstract*—A resonant texture allows the impedance of a metal surface to be changed from an electric conductor to a magnetic conductor, or any boundary condition in between. Varactor diodes incorporated into the structure allow electronic control the reflection phase and the surface wave properties. This tunable textured surface is used as an electronically steerable leaky wave antenna, by coupling energy into a leaky wave band, and tuning the surface to change the radiation angle. With a simple optimization algorithm, the beam can be electronically scanned over a wide range in both the forward and backward directions. Because the surface geometry provides multiple degrees of freedom per half wavelength, it allows independent control of the magnitude and phase of the surface wave radiation, so the antenna can be programmed to have a large effective aperture over the entire scan range. Radiation in the backward direction can also be understood in terms of a backward band, which can be measured directly from the surface reflection properties.**

## I. Introduction

THE USE of texture to modify the electromagnetic properties of a metal surface has a variety of applications. For example, materials known as soft and hard surfaces [1], that are made of one dimensionally periodic lattices of shorted waveguides or periodic strips, can be used to control the diffraction around metal objects [2], or as a coating inside waveguides and horns to modify the field profile within those structures [3]. These are related to corrugated surfaces, which have been studied extensively [4]–[8]. Two-dimensional (2-D) structures have also been built as arrays of waveguides [9] or metal rods [10]. Related materials known as high-impedance surfaces [11], [12] can serve as a substrate for low-profile antennas [13]. All of these materials rely on a common principle- a metal surface is coated with resonant structures that change the electromagnetic boundary condition of that surface. The resonant structures can take a variety of forms, including quarter-wavelength shorted waveguides, or inductive and capacitive regions that act as lumped resonant circuits. In most cases, the resonant structures are fine-grained, with a period that is much less than the wavelength of interest. We may refer to this general class of materials as textured surfaces.

By incorporating tunable structures or devices into textured surfaces, their capabilities are expanded to include active control of electromagnetic waves. For textured surfaces based on lumped resonant circuits, it is usually easer to tune the capacitance than the inductance. This can be accomplished using mechanical structures such as movable plates [14], or electrical components such as varactor diodes [15]. With a tunable textured surface, one can build devices such as high power waveguide phase shifters [16], and programmable reflectors that can steer or focus a reflected microwave beam [15]. The latter can provide a low-cost alternative to traditional electrically scanned antennas (ESAs) where phase shifters and complicated feed structures are replaced by a planar array of varactor diodes and a free space (quasioptic) feed. Despite being low-cost, these steerable reflector antennas are ruled out for many applications because they are not entirely planar. An alternative is to use a leaky wave design, where a wave is excited directly in the surface, and radiates energy into the surrounding space. By tuning the surface, the radiation can be steered. This concept has been demonstrated with a mechanically tuned surface [17], and the electronic equivalent is the starting point of the present study.

The simplest method of leaky wave beam steering is to tune the entire surface uniformly, which shifts the surface wave bands, and changes the wave vector of the radiated beam. However, as will be described below, this method is limited to scan angles in the forward direction from the feed, and the effective aperture is constrained by exponential decay of the surface waves. An improved method, which is the focus of this paper, involves programming the surface with a quasiperiodic impedance function that scatters the surface wave into free space. This has two benefits: 1) the scattered radiation can be steered over a wide scan range in both the forward and backward directions, and 2) the decay rate of the surface waves can be controlled independently of the beam angle to provide large effective aperture. In this paper, we compare the uniform and quasiperiodic steering methods, and examine ways for producing wide scan range and large effective aperture. The characteristics of backward leaky wave bands are also explored using reflectivity data.

## II. High-Impedance Surfaces

A flat metal conductor has low electromagnetic surface impedance, by definition. However, by applying a resonant texture, its impedance can be transformed to nearly any desired value. One example of such a texture is a lattice of small mushroom-shaped protrusions made of metal plates, connected to a common ground plane by vertical metal pins. These structures are often called high-impedance surfaces, or artificial magnetic

Manuscript received October 28, 2003; revised September 29, 2004.

The author is with the HRL Laboratories LLC, Malibu, CA 90265 USA (e-mail: dfsievenpiper@hrl.com).

Digital Object Identifier 10.1109/TAP.2004.840516

conductors. They are described in detail in the [11], [12], but a short summary of their properties is provided here for background. They are typically constructed as printed circuit boards, with metal plates on the front side connected to a ground plane on the back by metal plated vias. Such a structure can be described in terms of its capacitance *C*, due to the proximity of the neighboring plates, and its inductance *L*, determined by the thickness. The surface impedance is that of a lattice of parallel resonant *LC* circuits, which is

$$Z_s = \frac{j\omega L}{1-\omega^2 LC}. \tag{1}$$

Near its resonance frequency

$$\omega_0 = \frac{1}{\sqrt{LC}}, \tag{2}$$

its surface impedance is much greater than the impedance of free space, $\eta = 377\ \Omega$, and it reflects electromagnetic waves with zero phase shift, in contrast to an electric conductor, which reflects with a phase shift of $\pi$. At the resonance frequency it can be considered as an artificial magnetic conductor. Far from resonance it behaves as an ordinary electric conductor. Its reflection phase varies smoothly from $\pi$ to 0 to $-\pi$ as the frequency of the incident wave is tuned upward through $\omega_0$. Although these structures are often called high-impedance surfaces, the present work takes advantage of a broader range of properties, including nonuniform surface impedance, so we will refer to them simply as textured surfaces.

This type of textured surface has unique surface wave properties that allow it to be used as a steerable leaky wave antenna. Below resonance the surface is inductive, and it supports transverse magnetic (TM) surface waves. Above resonance it is capacitive, and supports transverse electric (TE) surface waves. Both of these waves are bound to the surface, and their fields decay exponentially into the surrounding space. Between the TM and TE bands lies a gap, where bound surface waves are not supported. The fractional bandwidth of the gap is

$$B = t\frac{2\pi}{\lambda_0} \tag{3}$$

where $t$ is the thickness of the surface, and $\lambda_0$ is the wavelength at resonance [15]. Although the surface does not support bound surface waves within the band gap, it does support TE polarized leaky waves, which radiate energy into the surrounding space as they propagate. These waves are the basis of the steerable leaky wave antennas described below.

## III. Tunable Textured Surfaces

By incorporating tunable elements such as varactor diodes into the high-impedance surface, its surface impedance and surface wave properties can be tuned, as a function of frequency. Although this work focuses on the mushroom-type high-impedance surface, many of the resonant textured surfaces described in the introduction could produce similar results. The benefits of this particular structure are that it has 2-D periodicity, which enables 2-D scanning, and it has vertical

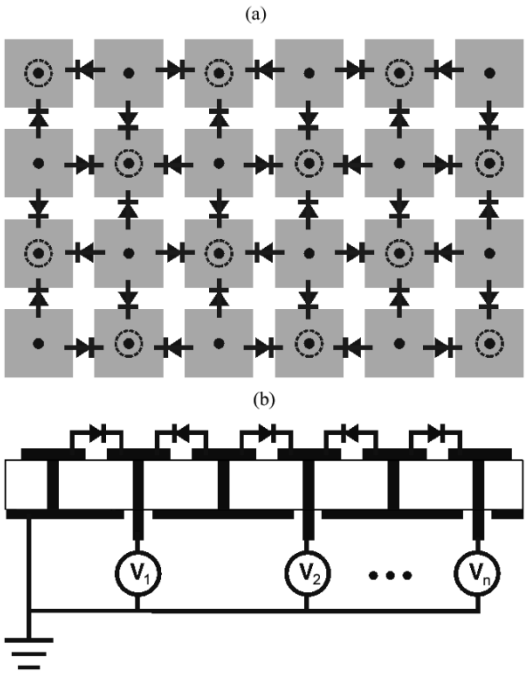


Fig. 1. (a) Top view and (b) side view of a tunable textured surface. It is built as a printed circuit board, where metal plates are arranged in a square lattice on the front side of the board, and are coupled to their neighbors by varactor diodes. Half of the plates are connected to a ground plane on the back by metal plated vias, and the other half are connected to bias lines that control the varactors.

metal vias, which provide a simple way to bias the varactors from the back side without affecting the microwave properties on the front.

The tunable surface used for this work consists of a lattice of square metal plates with varactor diodes connected between each adjacent pair, as shown in Fig. 1. It is built as a multi-layer circuit board, with three metal layers and two dielectric layers. The dielectric layers are both 1.6 mm thick Rogers Duroid 5880. The front metal layer contains the lattice of square plates, the middle layer is the ground plane, and the back layer contains the bias lines that control the varactors. The plates are 9.2-mm wide, with a 10-mm period. The surface measures 25-cm square, for a total of 625 individual plates. Half of the plates are connected to the ground plane by metal vias, and the other half are attached to the bias lines, in a checkerboard pattern.

The diodes are Micrometrics silicon hyperabrupt varactors, model MHV500-19-1, which have a usable capacitance range of roughly 0.2 to 0.8 pF. They are arranged in opposite directions on every alternate row and column, so that they are all reverse biased when a positive voltage is applied to the bias lines. The board contains a total of 1152 varactors. To simplify the circuitry, the diodes are biased in rows, using only 25 bias lines. Each plate could be tuned individually by using schemes such as row-and-column addressing.

By tuning the bias voltage from 0 to 20 V, the resonance frequency can be tuned over a range of about 2.5 to 4.5 GHz. Higher resonance frequencies can be achieved with this structure by applying two alternate voltages to adjacent rows, which doubles the effective lattice period, and forms an additional backward band that can extend beyond 5 GHz. The properties of backward bands will be discussed in a later section. For more

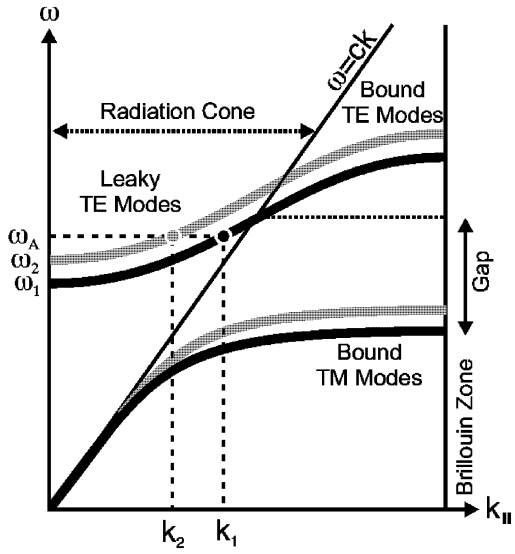


Fig. 2. Band diagram for surface waves on a tunable textured surface. When a wave is excited at a fixed frequency, its wave vector depends on the resonance frequency of the surface. If the resonance frequency is tuned from $\omega_1$ to $\omega_2$, the bands are shifted upward from the black curves to the gray curves. For a wave excited at $\omega_A$, the wave vector is tuned from $k_1$ to $k_2$, and the radiation angle is steered according to (4).

information on this particular structure including the reflection phase and magnitude for various voltages, it is described in detail in a previous publication [15], where it is used as an electronically steerable reflector.

## IV. Steerable Leaky Waves

Textured surfaces in general have frequency-dependent surface wave characteristics. At some frequencies, these surface waves radiate energy into the surrounding space as they propagate, and they are known as leaky waves. Many structures support such waves, and they have been used to build leaky wave antennas in a wide variety of different geometries, such as either longitudinal [18], [19] or transverse metal strips [20], [21], or the inverse structures such as longitudinal [22] or transverse slots. [23] Two-dimensional periodic structures have also been built using arrays of patches [24] or apertures [25]. Other kinds of leaky wave antennas are built using dielectric waveguides [26], [27].

For the structure used in this work, a band gap centered at the resonance frequency separates a lower TM band from a higher TE band. Within the gap, the textured surface supports leaky TE waves, which radiate into the surrounding space as they propagate along the surface. In Fig. 2, these leaky waves are indicated in the lower portion of the TE band that falls within the radiation cone, bounded by the line $\omega = ck_{||}$. Further details on the surface wave behavior of this structure, and the derivation of the curves in Fig. 2, are available in the [11], [12].

Radiation, or coupling between a space wave and a surface wave, requires that the wave vector of the space wave $k_0$, must have a component tangential to the surface that matches the wave vector of the surface wave $k_{||}$, as illustrated in Fig. 3. Radiation cannot occur when $\omega < ck_{||}$ because there is no angle $\theta$ for which this phase matching condition is satisfied. However,

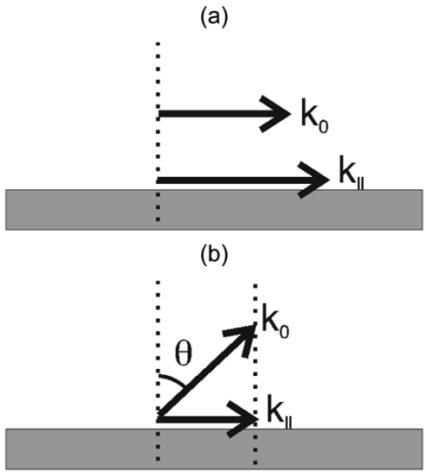


Fig. 3. Radiation requires that the wave vector of the space wave, $k_0$, must have a tangential component than matches $k_{||}$ of the surface wave. (a) If $k_{||} > k_0$, phase matching cannot occur for any angle, and the wave is bound to the surface. (b) For a leaky wave, the radiation angle $\theta$ is determined by phase matching at the surface.

when $\omega > ck_{||}$, energy can radiate from the surface into free space, at an angle given by

$$\theta = \sin^{-1}\left(\frac{ck_{||}}{\omega}\right). \tag{4}$$

We can take advantage of the relationship between radiation angle and surface wave vector, and the dispersion properties of the surface wave bands, to build an electronically steerable leaky wave antenna. Referring to Fig. 2, a wave is excited in the surface at a constant frequency, $\omega_{\mathrm{A}}$, as the resonance frequency is tuned from $\omega_1$ to $\omega_2$, to shift the surface wave bands vertically. When the resonance frequency is $\omega_1$, the excited mode has wave vector $k_1$, and radiates at an angle $\theta_1$ as determined by (4). When the surface is tuned to $\omega_2$, the entire TE band is shifted upward, so the excited mode has wave vector $k_2$, and the beam radiates at $\theta_2$. Modes near $k_{||} = 0$ radiate perpendicular to the surface, while modes near $k_{||} = \omega/c$ radiate at a grazing angle, so in principle, such an antenna could be steered from 0° to 90°, although in practice it is difficult to excite modes at the extremes of this range.

Leaky TE waves can be excited using a horizontally polarized feed, such as the flared notch antenna shown in Fig. 4. The feed can be placed very close to the surface, typically $\lambda/50$ or so, as long as it does not detune the surface by capacitive loading. Fig. 5 shows radiation patterns at 3.0 GHz for bias voltages ranging from 6 to 15 V, which corresponds to radiation angles ranging from 10° to 50°. As the voltage is increased, the capacitance of the varactors is decreased, which raises the resonance frequency of the textured surface, and shifts the TE band upward. The wave vector of the leaky wave is shorter for a fixed excitation frequency, so the radiation is closer to normal. Conversely, lower voltage results in radiation closer to grazing. For this simple antenna, the gain ranges from about 2 to 6 dBi, and the 3 dB beam width is about 40° for each case.

When a single tuning voltage is applied to the entire surface, the leakage rate is inversely related to the radiation angle. Modes near $k = 0$ radiate nearly normal to the surface, and the leaky

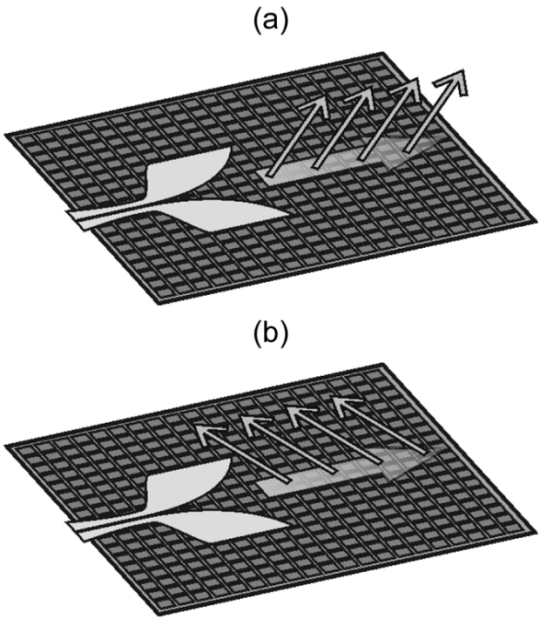


Fig. 4. Horizontally polarized flared notch antenna is an efficient feed for TE surface waves. This feed can launch (a) forward leaky waves or (b) backward leaky waves. In backward leaky waves, the surface wave still propagates away from the feed, but it radiates in the opposite direction.

wave is rapidly attenuated along the surface. Modes near the light line ($\omega = ck$) radiate at near grazing angles, and the wave is only gradually attenuated along the surface. The attenuation constant of leaky waves on textured surfaces, as determined by both quasianalytical calculations and computer simulations, is discussed in greater detail in previous publications [11], [12]. On a finite-length surface, leaky waves at near-grazing angles can reach the edge of the surface, and the resulting scattered radiation produces additional lobes, as seen in Fig. 5(d) and (e). This problem can be minimized by using a longer surface, or by using a nonuniform tuning method, as described in the next section.

With this simple uniform steering method, the operating frequency must be chosen so that the wave vector varies from nearly normal to nearly grazing over the tuning range of the varactors. If the operating frequency is too low, it will fall outside the TE band, or even within the TM band, which would require a different type of feed, and is nonetheless unsuitable for beam steering with this method. If it is too high, it will fall within the bound portion of the TE band. In that case, the results are unpredictable, since the bound waves propagate across the surface without radiating, and then scatter from the various edges of the surface with different phases. However, in the following section we will explore how these surface waves can be controlled through periodic scattering, to produce a much more versatile electronically steerable antenna.

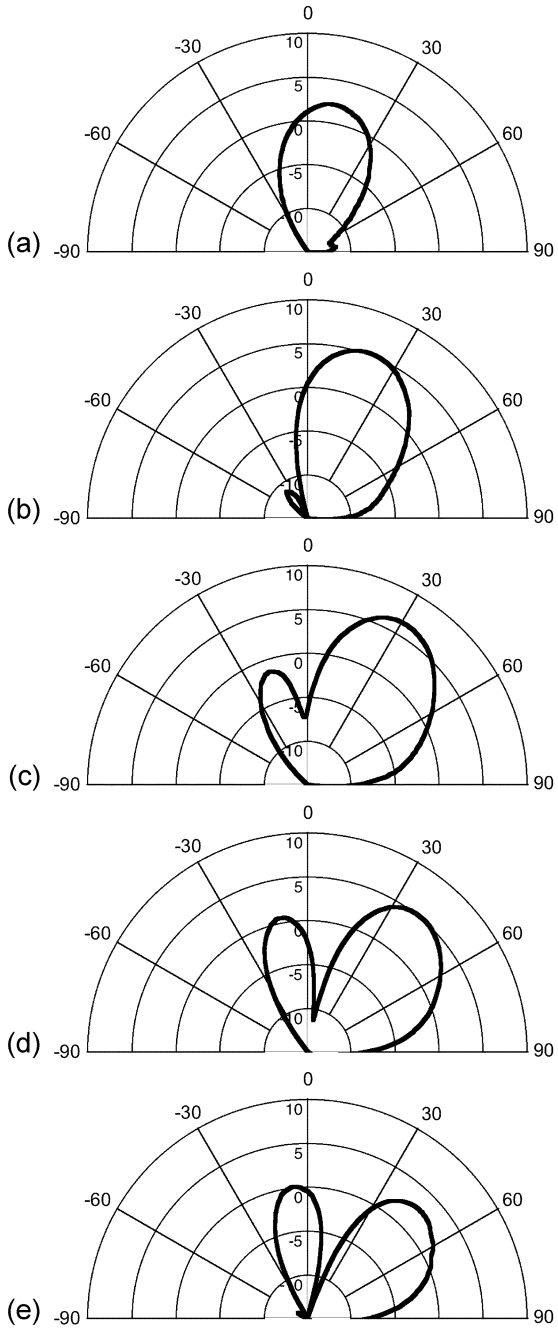


Fig. 5. Radiation patterns from leaky waves on a tunable textured surface at 3.0 GHz using the uniform tuning method. The voltage on all varactors in each case was (a) 15, (b) 12, (c) 9, (d) 7, and (e) 6 V. Lower voltage on the varactors results in larger capacitance, which lowers the resonance frequency of the surface, and pulls the TE band downward. This increases the wave vector for a fixed excitation frequency, so the beam is steered closer to the horizon.

## V. Nonuniform Surfaces

Although the uniform tuning method described above is capable of steerable radiation, it provides only limited scan range and effective aperture. In previous work on this surface for reflective beam steering [15], it was found that the radiation pattern could be significantly improved by applying a simple optimization technique. The same technique can be used to improve the gain and beamwidth of this leaky wave antenna, and to allow both forward and backward steering.

The surface is first rotated to the desired beam angle with respect to a fixed receive horn, then the voltage on each row is adjusted to optimize the transmitted power at that angle. All of the rows begin with the same voltage $V$, and each control line is

dithered by a sequentially smaller voltage $e$, until the received power does not change. The optimization technique is summarized as follows: 1) Apply a voltage $V$ to each row 0 through 24 of the surface. 2) For a single row $n$, adjust the control voltage to three values: $V, V+e, V-e$, and record the received power in each case. 3) Choose the voltage corresponding to the highest received power, and set $V(n)$ to that value. 4) Repeat for all rows until no further increase in received power is seen. 5) Reduce the incremental voltage e and continue to repeat for all rows until e is negligible, and the received power stops changing with further changes in $V(n)$. After the optimum control voltages are determined, the resulting radiation pattern is measured.

The varactors have a tuning range of 0 to 20 V, so 10 V was chosen as the starting voltage $V$, and the incremental voltage $e$ was set to values of 5, 2, 1, 0.5, 0.2, and 0.1 V, although other values produced similar results. The received power would typically converge within about 50 iterations, or about eight cycles through all rows for each value of $e$. Fig. 6 shows radiation patterns in which the surface has been optimized for angles ranging from 10° to 50 °. Comparing these results to those in Fig. 5, the gain obtained with optimized control voltages is about 8–10 dB, or about 5 dB higher on average than for uniform control voltages. The beam width is also significantly reduced compared to the uniform tuning case. It should be noted that the only criterion used in the optimization algorithm is the gain of the main beam, so no attempt has been made to reduce the sidelobes. For the plots shown in Fig. 6, the sidelobes vary in magnitude from about 5 to 13 dB below the main beam, and the variation was due to random differences in the final state of the optimization algorithm. Because some patterns had low sidelobes simply by chance, such as the 40° case in particular, it is possible that a more complicated optimization algorithm could be used to lower the sidelobes over the entire scan range. Furthermore, although the surface used in these experiments was only addressed by rows, all of the cells could be addressed individually for 2-D optimization, to improve the gain and allow 2-D steering. Finally, while this method does not attempt to optimize the input impedance of the antenna directly, optimizing the radiated power in the desired direction implicitly affects the input impedance. Therefore, it is likely that the input match plays a significant role in the control voltages for rows near the feed. However, further study is needed to assess the input impedance, as well as its variation with frequency.

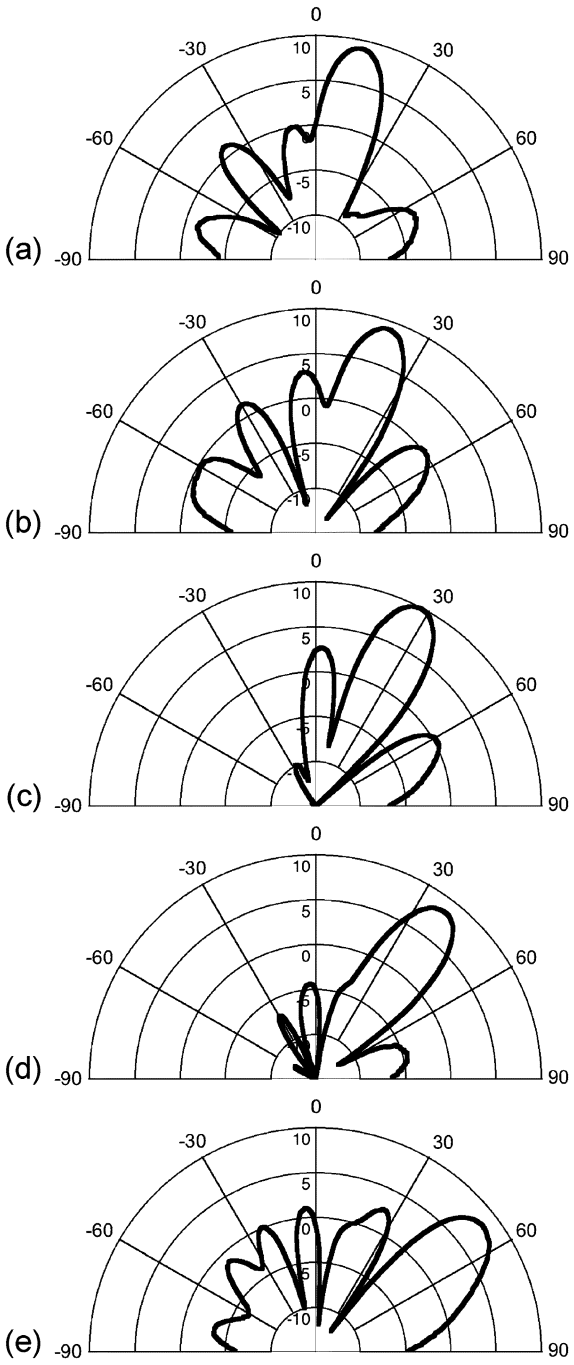


Fig. 6. Radiation patterns at 4.5 GHz for nonuniform control voltages. The surface is optimized for (a) 10°, (b) 20°, (c) 30°, (d) 40°, (e) 50°. This method produces higher gain and narrower beam width than the uniform tuning method. Sidelobe levels were not included in the optimization algorithm, so they varied randomly with each pattern. Since some cases such as 40° had low sidelobes by chance, it is expected that a more complicated optimization algorithm could likely improve the sidelobes for all patterns.

## VI. Backward Leaky Waves

Using the method described above, it is also possible to steer the beam directly to normal, or even in the backward direction, as shown in Fig. 7. In all, the steering range for this leaky wave antenna spans from $-50°$ to 50°. For backward leaky waves, the energy still travels outward from the source, so its group velocity is in the forward direction, but its phase velocity, which determines the radiation angle, is in the backward direction. Leaky wave structures capable of backward or broadside radiation have been studied extensively [28], including those that use magnetic materials [29], [30] arrays of multiple slots or obstacles [31], or other more complicated structures [32]. This antenna is unique because it can be electronically reconfigured to steer continuously from the forward to the backward direction at a single frequency. The average gain for the backward patterns is about 7 dBi, or about 2 dB lower than for the forward direction. The sidelobes are somewhat higher than in the forward steering cases, at about 5 dB below the main beam. However, in both cases this could potentially be improved, because the control voltages have not been optimized for low sidelobes. In all cases, the optimized nonuniform tuning method produced

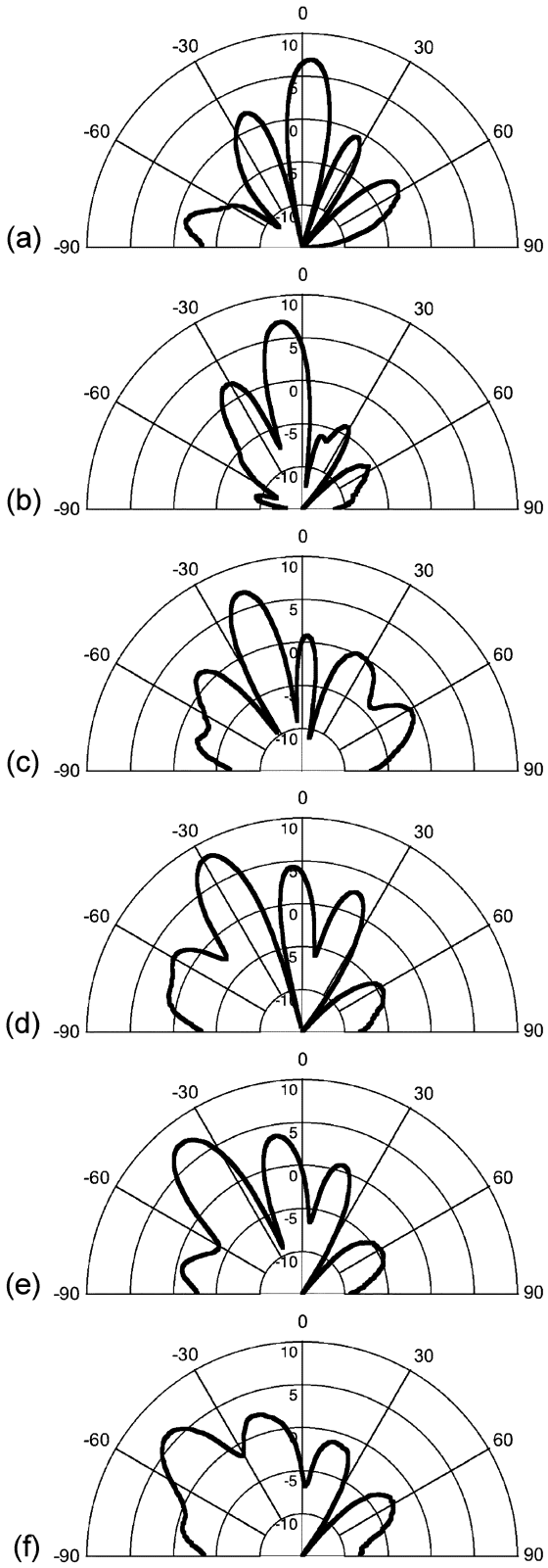


Fig. 7. Radiation patterns for the surface optimized for (a) normal radiation, to 0°, or backward radiation to (b) −10°, (c) −20°, (d) −30°, (e) −40°, (f) −50°. For backward radiation, the leaky wave still travels outward from the feed, but it radiates toward the opposite direction.

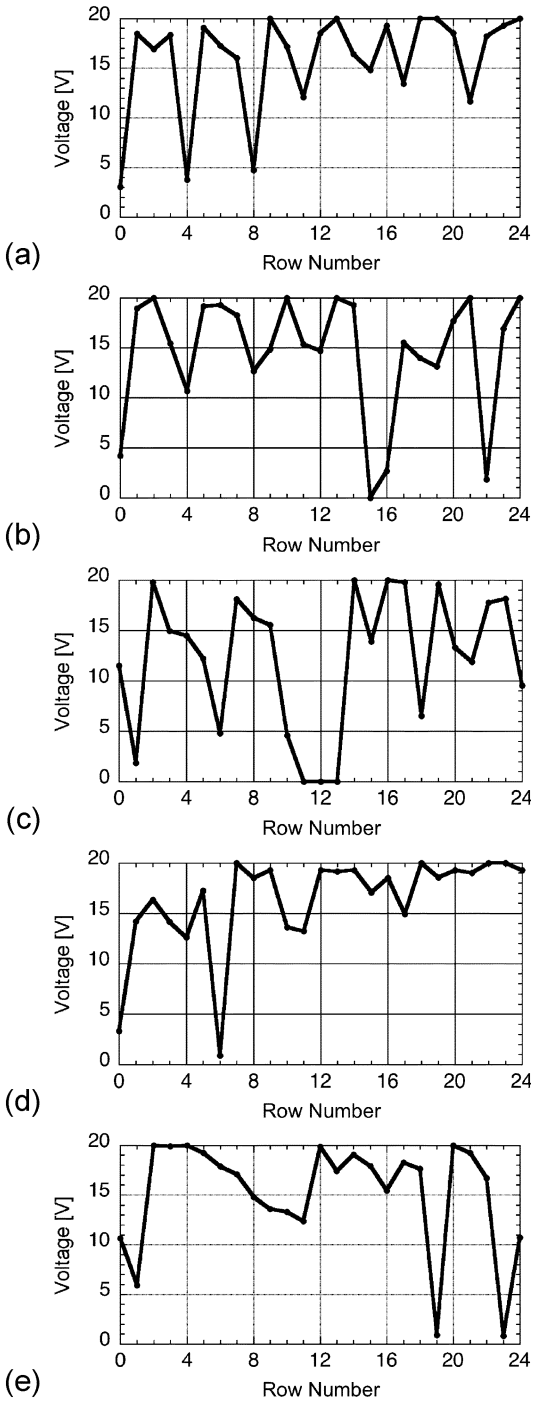


Fig. 8. The control voltages determined by the optimization algorithm for steering to (a) −40°, (b) −20°, (c) 0°, (d) 20°, (e) 40°. In each plot, the voltage is quasiperiodic, and surface waves are scattered into free space by this periodicity. About six periods can be seen for −40°, and about two periods for 40°.

higher gain and narrower beam width than the uniform tuning method.

The generation of backward leaky waves can be understood by examining the control voltages produced by the optimization algorithm. Fig. 8 shows examples for several beam angles ranging from − 40° to 40°. The common feature among these plots is that the control voltages are quasiperiodic, with a periodicity that depends on the beam angle. About six periods are visible for − 40°, and about two periods for 40°. Because the

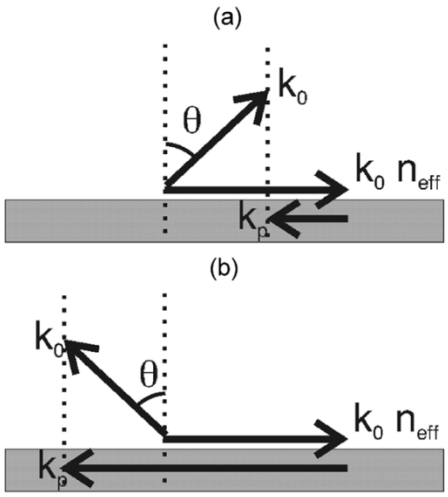


Fig. 9. Radiation requires phase matching between the wave vectors of the surface wave $k_0 n_{\text{eff}}$, the surface impedance function $k_p$, and the tangential component of the free space wave $k_0$. (a) If $k_p < k_0 n_{\text{eff}}$, the surface wave is scattered into free space in the forward direction. (b) If $k_p > k_0 n_{\text{eff}}$, the wave is scattered backward.

surface impedance is a nonlinear function of the control voltages on the varactors, the magnitude of the individual voltages does not provide as much information as the overall shape of the voltage function, so we consider only the most significant Fourier component for the following analysis. The other components play a role in the effective aperture, and will be discussed later.

When waves propagate across the surface, they are scattered by the nonuniform surface impedance. The scattered energy radiates at an angle determined by the wave vector of the surface wave, and the periodicity of the control voltages. The radiation angle may be determined by assuming that that a wave launched into the surface feels an effective refractive index of $n_{\text{eff}}$. Its wave vector is $k_0 n_{\text{eff}}$, where $k_0 = 2\pi\lambda$ is the free space wave vector. The surface impedance has period p, corresponding to a wave vector $k_p = 2\pi/p$. The scattered radiation in free space must have a total wave vector of $k_0$, and phase matching requires that it have a component parallel to the surface that is equal to the sum of the wave vectors of the surface wave and the surface impedance function. As illustrated in Fig. 9, the radiation is scattered into the forward direction if $k_p < k_0 n_{\text{eff}}$ and it is scattered backward if $k_p > k_0 n_{\text{eff}}$. In general, the radiation angle is

$$\theta = \text{Sin}^{-1}\left(\frac{k_0 n_{\text{eff}} - k_p}{k_0}\right). \tag{5}$$

In Fig. 10, the angle of the main beam is plotted versus the most significant Fourier component of $V(n)$. Equation (5) is fit to the data using the least squares method to find the implied refractive index, $n_{\text{eff}} = 1.2$. This value is within reason, considering that the substrate material has an index of 1.5 and the surrounding air has an index of 1.0.

## VII. Effective Aperture

Comparing Figs. 6 and 7 with Fig. 5, the quasiperiodic tuning method can produce not only a greater range of beam angles, but also a narrower beam with higher gain than the uniform

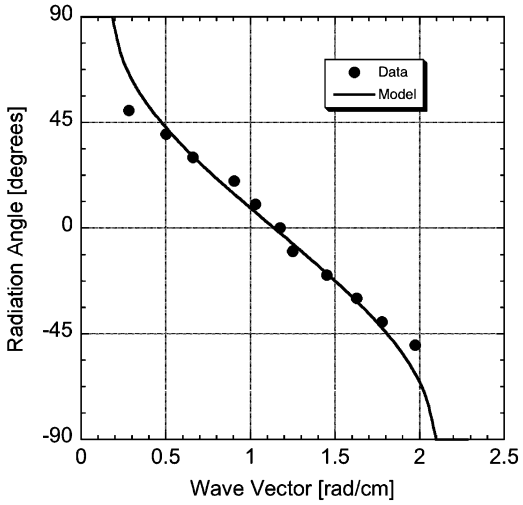


Fig. 10. The measured beam angle is plotted versus the most significant Fourier component of the applied voltage. The data is fit to (5) to determine the effective index seen by the surface waves, $n_{\text{eff}} = 1.2$.

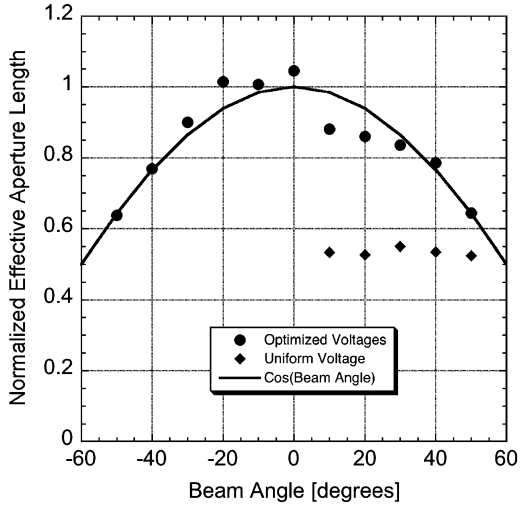


Fig. 11. The effective aperture, as determined by (6), normalized to the actual length of the surface, for both the uniform and quasiperiodic tuning methods. With the quasiperiodic steering method, the surface can be optimized so that the leaky waves fill the entire length of the surface, and it has the expected cosine dependence on beam angle.

tuning method. The effective aperture length can be estimated [33] from

$$L_{\text{eff}} \approx \frac{51\lambda}{W_{3\text{ dB}}}, \tag{6}$$

which is plotted in Fig. 11 for both the uniform and quasiperiodic cases, normalized to the actual length of the surface. For any large planar antenna, the effective aperture is expected to decrease by the cosine of the beam angle, because the surface appears smaller when projected at an angle. Based on the 3 dB beam width, the radiation patterns for the quasiperiodic surface imply an effective aperture nearly follows this ideal cosine curve, so the leaky waves appear to radiate from the entire length of the surface, about $3.75\lambda$ at 4.5 GHz, over the entire scan range of $-50^\circ$ to $50^\circ$.

The radiation patterns for the uniform voltage functions suggest that only about one-half of the surface is being used, for an

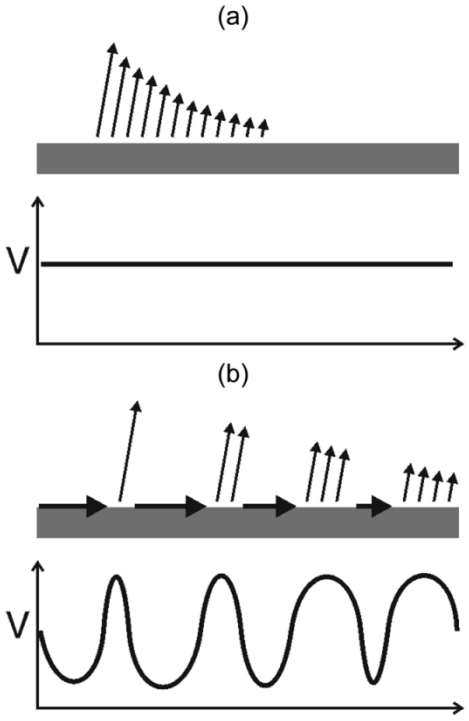


Fig. 12. The decay of a leaky wave for (a) the uniform tuning method, and (b) the quasiperiodic tuning method. The length of each arrow indicates the magnitude of the surface wave, and the number of arrows indicates the amount of radiation. The optimized surface can be considered to contain radiating regions and nonradiating regions, which allow the phase and magnitude of the leaky wave to be tuned independently.

effective aperture length of about $1.25\lambda$ at 3.0 GHz. The uniform case does not follow a cosine curve, and instead is roughly constant with beam angle. This is because for lower angles, the energy leaks out of the surface over a longer distance, which partially compensates for the smaller projected area.

Traveling wave antennas are commonly designed so that the leakage increases with the distance from the feed to compensate for the decay of the wave to create a uniformly filled aperture [34]. The same effect is achieved here by programming the textured surface with a quasiperiodic surface impedance. The most significant Fourier component of the surface impedance determines the angle of the main beam, while the other components affect the size and shape of the effective aperture.

To control both the radiation angle and the decay rate it is necessary to have two independently tunable parameters, yet the textured surface has only one - the bias voltage. This apparent inconsistency can be reconciled by recalling that there are several cells per half wavelength, about 3 in the structure described here, which provide additional degrees of freedom. As a simple model, the surface can be considered to contain separate radiating and propagating regions. We may associate the decay rate of the surface wave with the width of the radiating regions, and the radiation angle with the phase delay of the propagating regions between them. This concept is illustrated in Fig. 12. In order to change the beam angle and the decay rate independently, one could adjust the voltage in either the radiating regions or the propagating regions, respectively. The surface would still produce an ideal radiation pattern as long as the distance between radiating regions is at most one-half wavelength. This model is overly simple since the surface has only 3 cells per half wavelength, but it illustrates how it is possible to have independent control of both the radiation angle and the aperture profile with only a single tunable parameter, the control voltage. Based on the argument above, we may assume that independent control of both the magnitude and phase of the radiation requires a minimum of two cells per half wavelength, so the array is over-sampled by a factor of two.

The tunable textured surface is only one of several structures that can couple energy from a large area to a single feed. Recent work has shown that metal films patterned with a periodic texture are capable of producing a very narrow radiation pattern from a single sub-wavelength aperture, or alternatively of coupling light falling on a large area through the same small hole [35]–[39]. Other recent work has shown that periodic frequency selective surfaces can be used to greatly increase the effective aperture of an antenna placed beneath it. [40] These structures can all be considered as a class of planar lenses, which have the ability to focus energy onto a feed that is coplanar or nearly coplanar with the lens itself. Similarly, the tunable textured surface is a kind of steerable planar lens. Large arrays of such lenses could replace traditional phased arrays, where the signals would be distributed across the surface by leaky waves from a sparse array of feeds, and the surface itself would perform the electronic beam steering. Low-cost printed circuit boards and varactors could replace arrays of numerous transmit/receive modules, complex feed networks, and expensive assembly methods.

## VIII. Frequency Squint

Another measure of the antenna performance is the frequency squint, or change in beam angle with frequency. For leaky wave antennas, the same dispersion characteristics that provide beam steering also cause squint. As the frequency changes, so does the wave vector along the surface, so the radiation angle changes according to maintain the phase matching condition at the surface. This affects the usable bandwidth of the antenna, because broadband signals have a minimum beam width given by the squint, multiplied by the bandwidth of the signal. This effect is not limited to leaky wave antennas, and it occurs for any antenna that uses phase steering rather than true time delay steering. In this section, frequency squint is discussed for both beam steering methods, and the measured results are compared to expected values.

Frequency squint can be measured as the number of degrees that the beam angle changes, per Hertz of frequency offset. However, two antennas designed for two different frequencies cannot be compared directly with this method. Since an antenna would have the same performance if its dimensions and frequency were scaled, a more appropriate measure of squint is the change in angle per fractional bandwidth, which is simply the measured number of degrees per Hertz, multiplied by the operating frequency. This may be called the normalized squint $S$. Using this definition, the minimum beam width can be found for a given antenna geometry, scaled to any operating frequency. The squint is simply given by $S$, multiplied by the fractional bandwidth of the signal.

For the uniform tuning method, one can expect that the squint is highest for angles near normal, and lowest for angles near grazing, because the slope of the TE band increases with wave vector. In this case the squint is related to the inverse of the slope $dk/d\omega$, so it is greatest when the TE band is flat, near $k = 0$ (see Fig. 2). For the structure studied in this work, using the uniform tuning method, the normalized beam squint ranged from 204° to 108°, for beam angles ranging from near normal to near grazing. The average normalized squint was 137° over the scan range of 10° to 50°. This means, for example, that a signal with a fractional bandwidth of 1% would have a minimum beam width of about 1.37°. Because the frequency squint for the uniform tuning method depends entirely on the detailed shape of the dispersion curve, a theoretical analysis of this case is beyond the scope of this work.

For the quasiperiodic tuning method, the frequency squint is not related to the dispersion characteristics of the surface itself, to first order, so a theoretical analysis is possible without knowing the shape of the surface wave bands. It is worth noting that the quasiperiodic tuning method does not require the operating frequency to lie within the leaky wave region, over much of the surface. Radiation occurs because of scattering from the quasiperiodic surface impedance, which introduces coupling between the bound surface waves and the radiation modes [41]–[43]. The beam angle for this method is determined by the periodicity of the surface impedance function, $k_p$ in Fig. 9, and the phase velocity of the surface wave, $k_0 n_{\text{eff}}$. For each intended beam angle, $k_p$ is constant. Furthermore, $n_{\text{eff}}$ does not appear to vary significantly with beam angle, as indicated in Fig. 10 by the fact that the experimental data fits the model, which assumes that $n_{\text{eff}}$ is a constant. Thus, the squint arises primarily from the relationship between $k_0$ and frequency. By differentiating (5) with respect to frequency, and substituting $k_0$ for the intended beam angle, we obtain the normalized beam squint equation for the quasiperiodic tuning method

$$S = \frac{n_{\text{eff}} - \text{Sin}(\theta)}{\text{Cos}(\theta)}. \tag{7}$$

The squint depends only on the beam angle, and the effective index seen by the surface waves. By integrating (7) over $-50°$ to 50° using the measured value of $n_{\text{eff}} = 1.2$, the expected average normalized squint is 159°. The measured average frequency squint was 174°, which is close to the expected value. The discrepancy is probably due to the additional spatial frequency components in the surface impedance function besides $k_p$, that are present for aperture shaping, and are not included in the simple model given here. For both tuning methods, the beam angle increased (tilted further toward the positive direction) with frequency, which is consistent with the models shown in Figs. 3 and 9. It is worth noting that both methods described here had higher squint than the reflective steering method [15], by a factor of 1.5 to 2.0.

## IX. Measuring Backward Bands

In this section, we explore the properties of backward bands on textured surfaces, and study their behavior through reflection measurements. Consider a tunable textured surface in which alternate rows of plates are biased at two different voltages, low and high, as shown in Fig. 13. Dark and light gray regions between the plates indicate the resulting pattern of large and small capacitors. For a TE wave, the electric field is transverse to the direction of propagation, so it sees alternating capacitance as it propagates from row to row. Conversely, a TM wave sees columns of constant capacitance. For TE waves, the effective lattice period is doubled, and the Brillouin Zone [44] is halved, as shown in Fig. 14. The upper half of the TE band is folded into a reduced Brillouin zone, labeled BZ'. In the upper part of the TE band, the sign of the phase velocity $\omega/k$ is opposite to that of the group velocity $\partial\omega/\partial k$, so we may describe this as a backward band. The group velocity corresponds to the direction of energy propagation along the surface, which is always outward from the feed. The phase velocity, which determines the direction of radiation, progresses backward toward the feed.

Using mode analysis, the direction and relative strength of the electric field in the capacitors can be determined for various

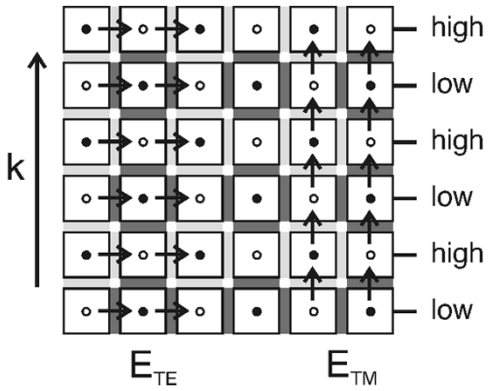


Fig. 13. Tunable textured surface, with alternating rows of varactors biased at low and high voltage. Filled circles in the center of the plates indicate vertical vias connected to a bias line, while open circles indicate a connection to the ground plane. Dark gray regions between the plates indicate large capacitance, and light gray regions indicate small capacitance. The electric field directions for both TE and TM waves are shown as small arrows.

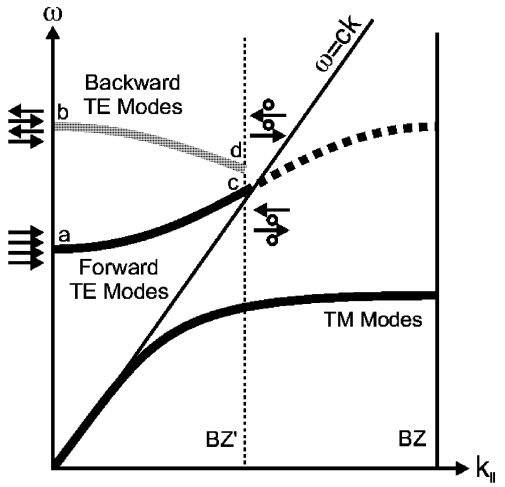


Fig. 14. Band diagram for a tunable textured surface with alternating rows of varactors biased at two different voltages. The TE band is folded into the reduced Brillouin zone BZ', and the upper portion corresponds to backward waves, where the phase velocity and group velocity are opposite. The electric fields in four rows are shown by small arrows, for four modes at the edges of the TE bands, labeled *a*, *b*, *c*, and *d*.

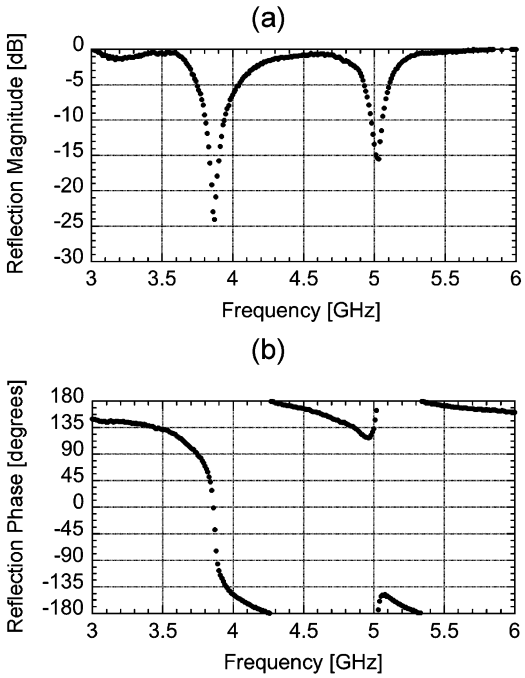


Fig. 15. The reflection (a) magnitude and (b) phase with alternate rows biased at 10 and 20 V. A backward band is formed, and the top of this band can be measured as a second resonance, which is visible in both plots.

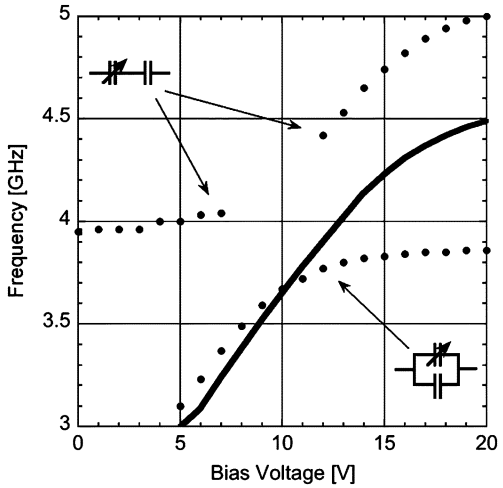


Fig. 16. Frequency of the two resonances when alternate rows are fixed at 10 V, and the other rows are tuned from 0 to 20 V. Measured modes for the dual-voltage case are plotted as black dots. For uniform voltage, the measured modes are plotted in a solid gray line, for reference. The two modes are associated with a parallel or series arrangement of capacitors in neighboring rows. The higher mode disappears near 10 V, as expected.

points on the band diagram. Groups of small arrows in Fig. 14 illustrate the electric field in four adjacent rows, for four states labeled $a, b, c$, and $d$. In the lowest frequency mode $a$, the electric field is parallel throughout the entire surface, just like the corresponding mode in a traditional high-impedance surface. In the next state with the same wave vector mode $b$, the fields are antiparallel in each adjacent row of capacitors. Because the capacitors have alternating values on every other row, the period of this mode matches that of the surface, and it lies at $k = 0$. To compare the frequencies of modes $a$ and $b$, consider a single pair of capacitors oriented along the direction of propagation. In mode $a$, the capacitors appear in parallel, because the voltage is the same across both of them. In mode $b$, the capacitors appear in series, because a continuous loop of current flows one way through the first one, and back the other way through the second one. For modes $c$ and $d$, one-half wavelength fits in each period of two capacitors. Thus, the field is zero in alternate rows of capacitors, and antiparallel in every other alternate row. The lower frequency mode $c$, lies entirely in the larger capacitors, while mode d exists only in the smaller capacitors.

It is possible to detect the presence of the backward band using reflection measurements. Modes at $k = 0$ are standing waves that support a finite tangential electric field at the surface, and they can be identified by frequencies where the reflection phase is zero, and by decreased reflectivity due to losses in the varactor diodes. When two different voltages are applied to alternate rows, two modes are visible, corresponding to the lower edge of the forward TE band, mode $a$, and the upper edge of the backward TE band mode $b$. This second mode is not present when a uniform voltage is applied to all of the varactors. In Fig. 15, which shows the reflection magnitude and phase when adjacent rows were biased at 10 and 20 V, modes $a$ and $b$ are visible at 3.9 and 5.0 GHz, respectively. Both modes can be tuned by adjusting the voltages on the odd or even rows, and their frequencies follow the expected trends, based on the model described above.

The behavior of modes $a$ and $b$ can be verified by biasing every other row of capacitors at a constant value of 10 V, and tuning the other rows from 0 to 20 V. In Fig. 16, the measured frequencies of the two modes are plotted as discrete points for each bias voltage. A solid gray line is also shown, corresponding to the resonant frequency of a uniformly tuned surface. The modes for the dual-bias cases behave as expected for two capacitors in series or parallel, where one of the capacitors is tuned. For example, the series case is dominated by the smaller of the two capacitors, while the parallel case is dominated by the larger. The two modes display an avoided crossing behavior, as expected. At 10 V, the lower mode coincides with the uniform voltage case, and the higher mode disappears, because all rows are nearly the same, so the second band vanishes.

A variety of related backward wave structures have been studied recently, and are also called negative index materials [45], [46]. By using textured surfaces as part of a parallel plate waveguide, other kinds of 2-D backward structures have been made [47]. By varying the shape of the unit cell, backward TM bands have also been created in open structures similar to the textured surface described here [48]. The direct measurement techniques and mode analysis described here can provide greater insight into structures of this type, and a broader theoretical foundation for forward and backward steerable leaky wave structures in general.

## X. Conclusion

A metal surface covered with a resonant texture can be transformed from an electric conductor to a magnetic conductor, or any impedance in between. Varactor diodes incorporated into this surface texture allow its reflection phase and its surface wave properties to be tuned electronically, and the surface can

be used as a low-cost, electronically steerable, antenna. A conformal feed can couple into a leaky TE band, and by tuning the surface, the TE band is shifted in frequency, which steers the radiated beam. This simple tuning method suffers from limited scan range, and small effective aperture, due to the decay of the leaky wave across the surface.

Using a quasiperiodic tuning method, the leaky wave antenna can be scanned over a wide range in both the forward or backward directions, and it can be programmed to have a large effective aperture. Although it is counterintuitive, independent control of both the beam angle and the effective aperture is possible with a single tuning voltage, because of the additional degrees of freedom provided by having at least two cells per half wavelength. This beam steering method does not rely on the dispersion properties of the surface, so the frequency squint is independent of the shape of the TE band. Finally, radiation to the backward direction can be understood in terms of a backward band, which can be measured directly from the surface reflection properties.

Using only printed circuit boards and varactors, this structure can provide a low-cost electronically steerable antenna, which can replace traditional alternatives containing multitudes of transmit/receive modules, bulky feed structures, and requiring costly assembly techniques. Additional work is required to examine full 2-D steering methods, symmetrical feed structures, and effective aperture limits for larger surfaces.

## ACKNOWLEDGMENT

The author would like to thank J. Schaffner for helpful discussions, J. J. Lee for providing the flared notch antenna used as the feed in these experiments, and M. Musni for help with fabrication and measurements.

## REFERENCES

[1] P.-S. Kildal, "Artificially soft and hard surfaces in electromagnetics," *IEEE Trans. Antennas Propag.*, vol. 38, no. 6, pp. 1537–1544, Jun. 1990.

[2] S. Maci, R. Tiberio, and A. Toccafondi, "Diffraction coefficients at edges in artificially soft and hard surfaces," *Electron. Lett.*, vol. 30, no. 3, pp. 203–205, Feb. 1994.

[3] E. Lier and P.-S. Kildal, "Soft and hard horn antennas," *IEEE Trans. Antennas Propag.*, vol. 36, no. 8, pp. 1152–1157, Aug. 1988.

[4] A. Harvey, "Periodic and guiding structures at microwave frequencies," *IRE Trans.*, vol. 8, p. 30, 1959.

[5] C. Elachi, "Waves in active and passive periodic structures: A review," *Proc. IEEE*, vol. 64, p. 1666, 1976.

[6] L. Brillouin, "Wave guides for slow waves," *J. Appl. Phys.*, vol. 19, p. 1023, 1948.

[7] W. Rotman, "A study of single-surface corrugated guides," in *Proc. IRE*, vol. 39, 1951, p. 952.

[8] R. Elliot, "On the theory of corrugated plane surfaces," *IRE Trans. Antennas Propag.*, vol. 2, no. 2, pp. 71–81, Apr. 1954.

[9] S. Lee and W. Jones, "Surface waves on two-dimensional corrugated surfaces," *Radio Sci.*, vol. 6, p. 811, 1971.

[10] R. King, D. Thiel, and K. Park, "The synthesis of surface reactance using an artificial dielectric," *IEEE Trans. Antennas Propag.*, vol. 31, no. 3, pp. 471–476, May 1983.

[11] D. Sievenpiper, "High-impedance electromagnetic surfaces," Ph.D. dissertation, Dept. Elect. Eng., University of California, Los Angeles, CA, 1999.

[12] D. Sievenpiper, L. Zhang, R. Broas, N. Alexopolous, and E. Yablonovitch, "High-impedance electromagnetic surfaces with a forbidden frequency band," *IEEE Transactions Microw. Theory Tech.*, vol. 47, no. 11, pp. 2059–2074, Nov. 1999.

[13] R. Broas, D. Sievenpiper, and E. Yablonovitch, "A high-impedance ground plane applied to a cellphone handset geometry," *IEEE Trans. Antennas Propag.*, vol. 49, no. 7, pp. 1262–1265, Jul. 2001.

[14] D. Sievenpiper, J. Schaffner, R. Loo, G. Tangonan, S. Ontiveros, and R. Harold, "A tunable impedance surface performing as a reconfigurable beam steering reflector," *IEEE Trans. Antennas Propag.*, vol. 50, no. 3, pp. 384–390, Mar. 2002.

[15] D. Sievenpiper, J. Schaffner, H. J. Song, R. Loo, and G. Tangonan, "Two-dimensional beam steering reflector using an electrically tunable impedance surface," *IEEE Trans. Antennas Propag.*, vol. 51, no. 10, pp. 2713–2722, Oct. 2003.

[16] J. A. Higgins, H. Xin, A. Sailer, and M. Rosker, "Ka-band waveguide phase shifter using tunable electromagnetic crystal sidewalls," *IEEE Trans. Microw. Theory Tech.*, vol. 51, no. 4, pp. 1281–1288, Apr. 2003.

[17] D. Sievenpiper, J. Schaffner, J. J. Lee, and S. Livingston, "A steerable leaky-wave antenna using a tunable impedance ground plane," *IEEE Antennas Wireless Propag. Lett.*, vol. 1, no. 10, pp. 179–182, Oct. 2002.

[18] P. W. Chen, C. S. Lee, and V. Nalbandian, "Planar double-layer leaky wave microstrip antenna," *IEEE Trans. Antennas Propag.*, vol. 50, no. 6, pp. 832–835, Jun. 2002.

[19] C.-N. Hu and C.-K. C. Tzuang, "Analysis and design of large leaky-mode array employing the coupled-mode approach," *IEEE Trans. Microw. Theory Tech.*, pt. 1, vol. 49, no. 4, pp. 629–636, Apr. 2001.

[20] J. W. Lee, J. J. Eom, K. H. Park, and W. J. Chun, "TM-wave radiation from grooves in a dielectric-covered ground plane," *IEEE Trans. Antennas Propag.*, vol. 49, no. 1, pp. 104–105, Jan. 2001.

[21] Y. Yashchyshyn and J. Modelski, "The leaky-wave antenna with ferroelectric substrate," in *Proc. 14th Int. Conf. Microwaves, Radar and Wireless Communications, MIKON-2002*, vol. 1, Gdansk, Poland, May 2002, pp. 218–221.

[22] J. H. Wang and K. K. Mei, "Theory and analysis of leaky coaxial cables with periodic slots," *IEEE Trans. Antennas Propag.*, vol. 49, no. 12, pp. 1723–1732, Dec. 2001.

[23] C.-C. Chen and C.-K. C. Tzuang, "Phase-shifterless beam-steering micro-slotline antenna," *Electron. Lett.*, vol. 38, no. 8, pp. 354–355, Apr. 2002.

[24] G. Broussaud, "A new antenna type of plane structure," *Ann. Radioelectricite*, vol. 11, pp. 70–88, 1956. French.

[25] T. Zhao, D. R. Jackson, and J. T. Williams, "Radiation characteristics of a 2d periodic slot leaky-wave antenna," in *Proc. IEEE Antennas and Propagation Soc. Int. Symp.*, vol. 1, San Antonio, TX, Jun. 2002, pp. 482–485.

[26] X.-Y. Zeng, K.-M. Luk, and S.-J. Xu, "A novel leaky NRD guide with a double-layer dielectric slab," *IEEE Trans. Microw. Theory Tech.*, pt. 1, vol. 49, no. 4, pp. 585–588, Apr. 2001.

[27] L. Huang, J.-C. Chiao, and M. P. De Lisio, "An electronically switchable leaky wave antenna," *IEEE Trans. Antennas Propag.*, vol. 48, no. 11, pp. 1769–1772, Nov. 2000.

[28] T. Tamer and F. Kou, "Varieties of leaky waves and their excitation along multilayered structures," *IEEE J. Quantum Electron.*, vol. 22, no. 4, pp. 544–551, Apr. 1986.

[29] P. Baccarelli, C. Di Nallo, F. Frezza, A. Galli, and P. Lampariello, "The role of complex waves of proper type in radiative effects of nonreciprocal structures," in *IEEE MTT-S Int. Microwave Symp. Digest*, vol. 2, Jun. 1997, pp. 491–494.

[30] A. Yakovlev and G. Hanson, "Leaky-wave dispersion behavior on a grounded ferrite slab waveguide," *IEEE Microw. Wireless Component Lett.*, vol. 12, no. 10, pp. 398–400, Oct. 2002.

[31] M. Guglielmi and D. Jackson, "Broadside radiation from periodic leaky-wave antennas," *IEEE Trans. Antennas Propag.*, vol. 41, no. 1, pp. 31–37, Jan. 1993.

[32] S.-G. Mao and M.-Y. Chen, "Propagation characteristics of finite-width conductor-backed coplanar waveguides with periodic electromagnetic bandgap cells," *IEEE Trans. Microw. Theory Tech.*, vol. 50, no. 11, pp. 2624–2628, Nov. 2002.

[33] C. Balanis, *Antenna Theory, Analysis, and Design*, 2nd ed, New York: Wiley, 1997.

[34] M. Takahashi, J.-I. Takada, M. Ando, and N. Goto, "A Slot design for uniform aperture field distribution in single-layered radial line slot antennas," *IEEE Trans. Antennas Propag.*, vol. 39, no. 7, pp. 954–959, Jul. 1991.

[35] R. Dragila, B. Luther-Davies, and S. Vukovick, "High transparency of classically opaque metallic films," *Phy. Rev. Lett.*, vol. 55, no. 10, pp. 1117–1120, Sep. 1985.

[36] T. Ebbesen, H. Lezec, H. Ghaemi, T. Thio, and P. Wolff, "Extrordinary optical transmission through sub-wavelength hole arrays," *Nature*, vol. 391, pp. 667–669, Feb. 1998.
[37] L. Martin-Moreno, F. Garcia-Vidal, H. Lezec, K. Pellerin, T. Thio, J. Pendry, and T. Ebbesen, "Theory of extraordinary optical transmission through subwavelength hole arrays," *Phys. Rev. Lett.*, vol. 86, no. 6, pp. 1114–1117, Feb. 2001.
[38] D. Jackson, T. Zhao, J. Williams, and A. Oliner, "Leaky surface plasmon theory for dramatically enhanced transmission through a sub-wavelength aperture II. Leaky-wave antenna model," in *Proc. Antennas and Propagation Soc. Int. Symp.*, vol. 2, Jun. 2003, pp. 1095–1098.
[39] Z. Sun, Y. Jung, and H. Kim, "Role of surface plasmons in the optical interaction in metallic gratings with narrow slits," *Appl. Phys. Lett.*, vol. 83, no. 15, pp. 3021–3023, Oct. 2003.
[40] S. Maci, R. Magliacani, and A. Cucini, "Leaky wave antennas realized by using artificial surfaces," in *Proc. IEEE Antennas and Propagation Soc. Int. Symp.*, vol. 2, Jun. 2003, pp. 1099–1102.
[41] A. Thomas and F. Zucker, "Radiation from modulated surface wave structures I," in *IRE Int. Convention Record*, vol. 5, Mar. 1957, pp. 153–160.
[42] R. Pease, "Radiation from modulated surface wave structures II," in *IRE Int. Convention Record*, vol. 5, Mar. 1957, pp. 161–165.
[43] A. Oliner and A. Hessel, "Guided waves on sinusoidally-modulated reactance surfaces," *IEEE Trans. Antennas Propag.*, vol. 7, no. 5, pp. 201–208, Dec. 1959.
[44] L. Brillouin, *Wave Propagation in Periodic Structures*. New York: McGraw-Hill, 1946.
[45] D. Smith, W. Padilla, D. Vier, S. Nemat-Nasser, and S. Schultz, "Composite medium with simultaneously negative permeability and permittivity," *Phys. Rev. Lett.*, vol. 84, no. 18, pp. 4184–4187, May 2000.
[46] D. Smith and N. Kroll, "Negative refractive index in left-handed materials," *Phys. Rev. Lett.*, vol. 85, no. 14, pp. 2933–2936, Oct. 2000.
[47] G. Eleftheriades, A. Iyer, and P. Kremer, "Planar negative refractive index media using periodically loaded L-C transmission lines," *IEEE Trans. Microw. Theory Tech.*, vol. 50, no. 12, pp. 2702–2712, Dec. 2002.
[48] L. Liu, C. Caloz, and T. Itoh, "Dominant mode leaky-wave antenna with backfire to endfire scanning capability," *Electron. Lett.*, vol. 38, no. 23, pp. 1414–1416, Nov. 2002.

**Daniel F. Sievenpiper** (S'95–M'98–SM'04) received the B.S. and Ph.D. degrees in electrical engineering from the University of California, Los Angeles, in 1994 and 1999, respectively.

He is currently a Senior Research Staff Scientist with HRL Laboratories, Malibu, CA, where he works in the field of electromagnetics, antennas, and wireless communication. His interests include novel electromagnetic materials, low-cost beam steering, RF MEMS for advanced antennas and radio front ends, and new communication system architectures. He has more than 15 U.S. patents and more than 40 refereed journal publications and conference papers.